

## Classical and quantum chaos in molecular rotational excitation by ac electric fields

N. Moiseyev<sup>1</sup>, H.J. Korsch<sup>2</sup>, B. Mirbach<sup>2</sup>

<sup>1</sup> Department of Chemistry, Technion-Israel Institute of Technology, Haifa 32000, Israel

<sup>2</sup> Fachbereich Physik, Universität Kaiserslautern, D-67663 Kaiserslautern, Germany

Received: 27 July 1993 / Final version: 13 October 1993

**Abstract.** The interaction of diatomic molecules with an ac electric field is described by a periodically driven rigid rotor model Hamiltonian. Numerical studies of the classical and quantum dynamics reveal a remarkably close correspondence between classically chaotic dynamics and quantum time evolution. Unlike the periodically kicked rotor all the quasienergy states located in the (bounded) chaotic region in phase space are extended states. Expanded in the free rotor basis, their coefficients fulfill the statistical predictions for random vectors. Consequently, even in off resonance condition the probability for transferring angular momentum to the diatomic molecule is large and eventually the first  $j_m$  excited rotational states will be “democratically” populated. The value of  $j_m$  is determined by the bounded chaotic region in phase space. The rotational occupation probability shows an erratic behavior with fluctuations following the statistical predictions for random quantum states.

**PACS:** 03.65.-w; 05.45.+b; 33.80.Be

### 1. Introduction

The interrelation of quantum and classical dynamics for systems which are chaotic in the classical limit is extensively studied (see, e.g., the textbooks by Gutzwiller [1] and Haake [2], the collection of articles on irregular atomic systems [3] and recent conference proceedings [4]). For time-independent Hamiltonians the main fingerprint of chaos is in the level statistics of bound states [5]. For systems with time-dependent Hamiltonians the classical chaotic motion can be bounded or unbounded in phase space. So far most of the studies were carried out for periodically kicked systems with unbounded classical motion in phase space. It was shown that in many such systems like a kicked planar rotor [6–11], surface-state electrons [12] and hydrogen atoms in monochromatic fields [13, 14], the classical chaos is suppressed in quan-

tum mechanics by a mechanism similar to Anderson localization in disordered solids [15] (note, however, that Anderson localization is *not* necessarily found for all kicked systems [16]). This type of quantum limitation of chaos is reflected in the exponential localization of the quasienergy states in the field-free energy (or momentum) space, even when the system is off resonance, i.e. for irrational values of the ratio between the rotor and the driving frequency. We have found recently that the dynamics of a periodically driven anharmonic oscillator, where the classical chaotic motion is bounded in phase space [17–19], is markedly different from kicked systems with unbounded classical chaotic motion in phase space [20]. As we demonstrate in Sect. II the dynamics of the periodically driven rotor is structurally very similar to the dynamics of the periodically driven anharmonic oscillator. In Sect. III we show that the quasienergy states of the periodically driven rotor – unlike the solutions of the kicked rotor – are extended states bounded only by the classical KAM-confinement [21, 22]. Consequently, even under off resonance conditions the probability for transferring angular momentum to the rotor is large and eventually the first  $j_m$  excited rotational states will be almost equally populated. The value of  $j_m$  is determined by the bounded chaotic region in phase space. As the chaotic region becomes larger, e.g. by varying the field intensity parameter,  $j_m$  is increased and the diatomic molecule can be found in higher excited states. It had already been pointed out by Blümel et al. [23] that under specific conditions an almost equal population of  $j$ -states up to some maximum value  $j_m$  is to be expected for such driven rotor systems. They did, however, not present results for the rotational distribution.

In Sect. IV the statistical properties of both the expansion coefficients of the quasienergy states in the free-rotor basis and the time-dependent excitation probabilities are analysed in more detail. The quasienergy states can be regarded as random orthogonal vectors in an  $N$ -dimensional *real* vectorspace ( $N \leq j_m$ ). The value of  $N$  is determined by the area of the chaotic region of phase space. The rotational occupation probabilities show an

almost random behavior as a function of time, which can be modelled by a random motion of the state vector on the unit sphere in an  $N$ -dimensional *complex* vector space. The observed quantum fluctuations are found to be in close agreement with statistical predictions.

The periodically driven rotor provides a reasonable model for field excitation of diatomic molecules and, as discussed in Sect. V, it is expected that the experimentally measured rotational energy spectra of diatomic molecules like CsI or PbTe under the influence of strong electromagnetic fields (e.g. strong Laser fields) will be chaotic.

## II. Classical dynamics of a periodically driven 2D rigid rotor

The Hamiltonian of our model in dimensionless units is given by

$$H(t) = \frac{J^2}{2} - f \cos \theta \cos \omega t \quad (1)$$

(note, that one of the two parameters,  $f$  and  $\omega$ , can be removed by rescaling, e.g.  $\omega t =: t'$ ,  $f\omega^{-2} =: f'$ ). The rotational momentum  $|J|$  is equivalent to  $\hbar j$  in quantum mechanics, where  $j$  is the rotational quantum number. The classical driven rotor (1) has been studied by several authors, both theoretically [24] and experimentally [25], modelling magnetic dipoles in oscillating magnetic fields studying almost exclusively the bifurcation properties of stable periodic orbits. On the other hand, Berman et al. [26] realized that this system can serve as a model for studying effects of overlapping resonances, thus being of fundamental interest. Rewriting Hamiltonian (1) as

$$H(t) = \frac{J^2}{2} - \frac{f}{2} (\cos(\theta - \omega t) + \cos(\theta + \omega t)), \quad (2)$$

one immediately recognizes two fundamental resonances with winding numbers  $\Omega(J_+) = \omega$  and  $\Omega(J_-) = -\omega$  lying symmetrically in the upper and lower  $J$ -halfplane, respectively. When one of the driving terms is neglected the system is integrable. For small values of the parameter  $f$  the width of the two resonances is small compared to their distance and perturb each other only slightly leaving the system almost integrable. Increasing the parameter  $f$  the widths of the resonances grow and the measure of the phase space occupied by chaotic trajectories increases. The Chirikov criterion [27] states that the transition to global stochasticity occurs when resonances overlap. Details about the overlap parameter for the system under investigation and the effects on the quantum dynamics of the system can be found in [26]. In the present calculations we will use  $f = 1$  and  $\omega = 1$ , where the resonances have clearly overlapped and the classical motion between the two resonances is almost entirely chaotic.

The classical dynamics is elucidated by the stroboscopic Poincaré section of phase space at times  $t = nT$  ( $T = 2\pi$  is the period of the driving force), which is represented in Fig. 1 (note that because of symmetry this and

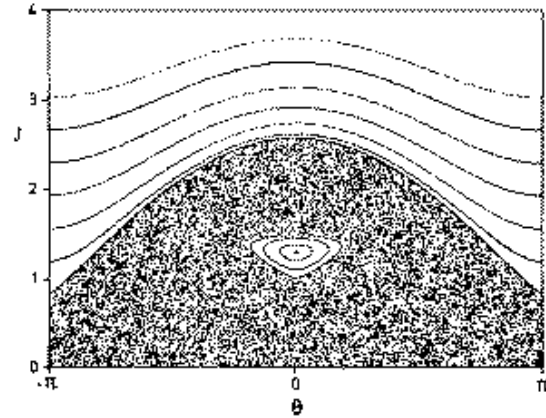


Fig. 1. Synoptic Poincaré section of classical phase space at  $t = nT$  ( $n = 0, 1, 2, \dots$ ). Only the upper region,  $J \geq 0$ , is shown because of symmetry. All points in the chaotic region result from a single classical trajectory

(the following graphs show only the positive  $J$ -region). The Poincaré section shows a large *bounded* chaotic zone obtained from following a single classical trajectory with a small embedded regular island which is the centre of the resonance mentioned above. The transition between the inner chaotic and the outer almost regular regime is extremely sharp as observed before for a class of continuously driven anharmonic oscillators [17–19, 28]. The outside regular region describes the rotating motion of a hindered rotor. Here the motion follows almost adiabatically the Hamiltonian (2) and the momenta at time  $t = nT$  are approximately given by  $J = J(\theta) = \pm \sqrt{2f} (\text{const} - \sin^2 \theta/2)$ , i.e. they have maximum or minimum values when the molecular axis is parallel to the direction of the field at this time. The inner regular island describes a rotor which exhibits at  $t = nT$  an almost periodic librational motion. In the center of the island at  $(\theta, J) = (0, 1.29)$  there is a stable  $T$ -periodic trajectory. Smaller island structures can be detected by closer inspection. The most prominent ones are a period-three chain appearing at  $(\theta, J) = (0, 2.10)$ ,  $(\pm 1.44, 0.71)$ ,  $(1.44, 0.71)$ , which are, however, not visible in Fig. 1. The chaotic sea, describes an erratic motion, where the angular momentum varies from 0 to 2.6. The shape of the chaotic sea shows that there is an almost equal probability of finding the erratic rotor at  $|J| < 0.8$ , and the probability is gradually reduced to zero as  $J$  approaches the value of 2.6. The size of the bounded chaotic region and of the inner regular one depends on the value of the parameter  $f$ . The details of the inner island structure are sensitive to  $f$  and show rich bifurcation phenomena when  $f$  is varied. For energies of the field-free Hamiltonian exceeding  $H_0 = 3.3$  (i.e.  $|J| > J_m = 2.6$ ) the dynamics is (almost) completely regular. Numerical integration provides a phase space area of  $\int J d\theta = 0.55$  for the inner regular island. The phase space area of the bounded chaotic region including the embedded stability island(s) yields a value of  $\int J d\theta = 12.06$ .

In order to study classical vs. quantum dynamics we calculated  $J(t)$  and  $\theta(t)$  as function of time for  $8 \cdot 10^3$  equidistantly distributed phase space points with  $J(t=0)$

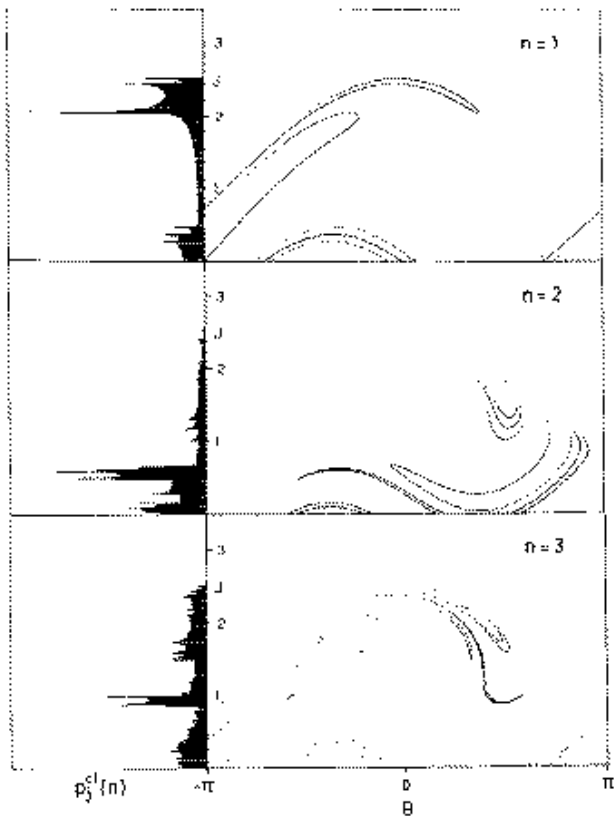


Fig. 2. Poincaré sections of classical phase space at  $t = nT$  ( $n = 1, 2, 3$ ) resulting from  $8 \cdot 10^3$  classical trajectories for initial values  $J(t=0) = 0$  uniformly covering the interval  $0 \leq \theta \leq 2\pi$ . On the left the classical probability distributions for excitation of the initially non-rotating rotor,  $p_j^{cl}(n)$ , are shown as histograms ( $j = J/h$  with  $h = 0.02$ )

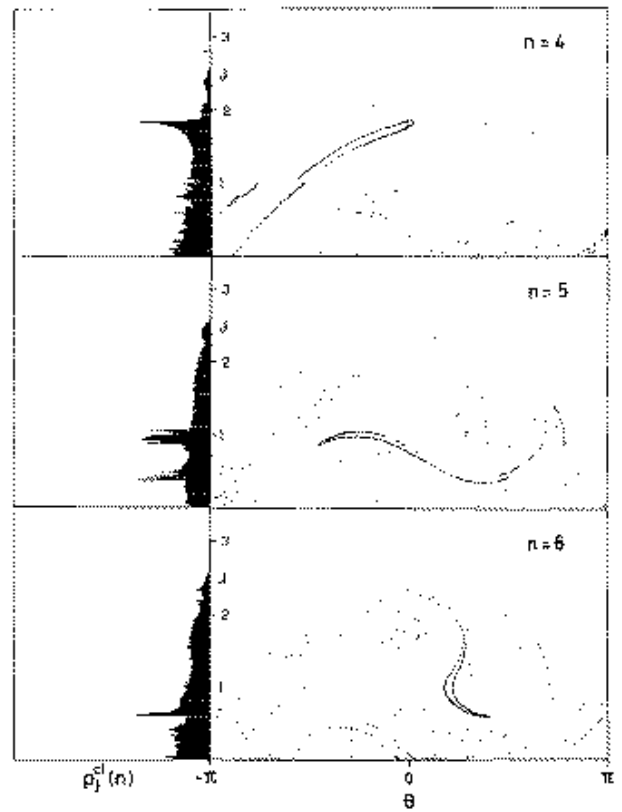


Fig. 3. Poincaré sections of classical phase space at  $t = nT$  ( $n = 4, 5, 6$ ) resulting from  $8 \cdot 10^3$  classical trajectories for initial values  $J(t=0) = 0$  uniformly covering the interval  $0 \leq \theta \leq 2\pi$ . On the left the classical probability distributions for excitation of the initially non-rotating rotor,  $p_j^{cl}(n)$ , are shown as histograms ( $j = J/h$  with  $h = 0.02$ )

$= 0$  in the interval  $0 \leq \theta \leq 2\pi$ . This classical calculation mimics a diatomic molecule in its rotational ground state, which is rotationally excited due to the interaction with a CW laser. The classical stroboscopic Poincaré section of phase space at times  $t = 2\pi n$  ( $2\pi$  is the period of the driving field) represented in Figs. 2–4 show the iterates of the initial curve  $\{\theta, J=0\}$  in the positive  $J$ -half of the cylindrical phase space during the first few time-periods,  $n = 1, \dots, 6$ , as well as in the asymptotic limit  $n \rightarrow \infty$ . In

addition, on the left hand side the probability  $p_j^{cl}(n)$  to find the classical rotor in state  $j$  (i.e. with rotational momentum in the interval  $(j < J(t)/h < j + 1)$  at time  $t = 2\pi n$  is shown as a histogram using a box-length of  $h = 0.02$  in order to compare with the quantum results below. Note, that these distributions are converged results based on a much larger number of classical trajectories, whereas in the corresponding phase space plots in Figs. 2–3 only 8000 initial points are used.

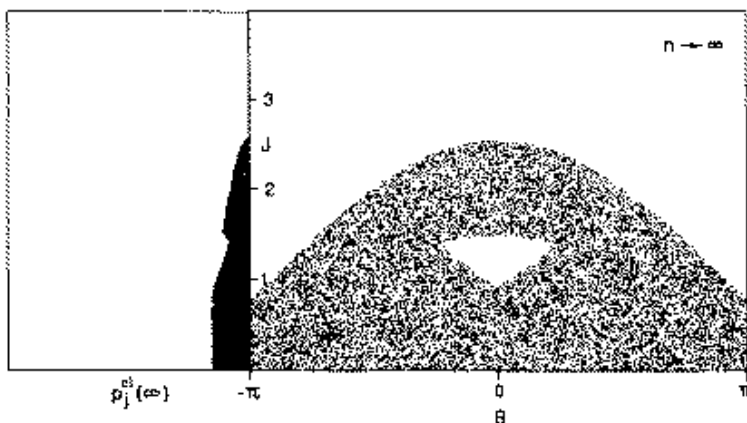


Fig. 4. The Poincaré section of classical phase space for  $t \rightarrow \infty$ . On the left the asymptotic classical excitation probability for an initially non-rotating rotor,  $p_j^{cl}(\infty)$ , is shown as a histogram ( $j = J/h$  with  $h = 0.02$ )

Several features of the classical excitation dynamics deserve discussion: First, we see that the initial distribution lies entirely inside the chaotic region and the iterates uniformly fill the chaotic sea with increasing number of periods  $n$ . The probability distribution rapidly approaches the asymptotic result, which is simply the projection

$$\rho_j^{cl} = \frac{1}{h} \int_{j/h}^{(j+1)/h} dJ \int d\theta \mathbb{1}_{\text{chaotic sea}} \quad (3)$$

of the area of the chaotic sea shown in Fig. 1 onto the discretized  $J$ -axis, normalized as

$$\sum_j \rho_j^{cl} = \frac{A}{h} \approx N. \quad (4)$$

We find  $p_j^{cl} = \rho_j^{cl} h/A$  to be almost constant for  $0 < J < 0.9$  ( $0 \leq j \leq 45$ ) and decreasing to zero at  $J_m = 2.6$  ( $J_m = J_m/h = 130$ ) (see Fig. 4). Clearly visible in the distribution is the large stability island reducing the probability. The tiny dip close to  $j = 36$  is due to small period-3 islands which are hardly visible in the surface of section.

Second, during the first few excitation periods pronounced structures in the rotational excitation probabilities are observable. These are due to horizontal projections of  $J = J(\theta, n)$ , which is the curve of  $n^{\text{th}}$  iteration of the initial point at a rotor orientation  $\theta$ , producing square root singularities in the classical excitation probability (note, that the singularities are smoothed by taking histograms). Such singularities are well known in the field of collisional rotational excitation of molecular or nuclear targets and widely known as rotational rainbows (for details see, e.g., the reviews [33]) and  $J(\theta, n)$  is known as the rotational excitation function. For collisional systems this excitation function typically shows only a small number of maxima, depending on the topology of the interaction potential and the number of impacts, whereas in the present case the number of rotational rainbows is much larger and increases exponentially fast with  $n$ . After  $n = 5$  periods the rainbows are no longer clearly distinguishable from each other with exception of one or two which are still dominant (see below). For  $n > 10$  the structure is already very similar to the long-time limit. A rough

estimate of the proliferation of the rotational rainbows is immediate. Let us recall that the classical chaotic spreading is roughly determined by a single number, namely the Lyapunov exponent  $\lambda$ , which has been computed numerically as  $\lambda = 1.065$  in the present case. Propagating a closed curve in time (e.g. the line defined by  $J=0$ ) it is subsequently stretched and folded and its length,  $L$ , grows exponentially in time as  $L_n = L_0 e^{\lambda n}$ . In our case where the spatial extension of phase space is  $2\pi$  the number of rainbows generated by the curve is roughly given by the number of sheets,  $L/2\pi$ , i.e. by  $e^{\lambda n}$  at time  $2\pi n$ . This yields an estimated number of 205 rainbows after  $n = 5$  optical cycles, half of them lying in the upper momentum plane. For the value of  $h = 0.02$  used in the quantum computations below there are only 130 different rotational momentum states (in classical considerations: boxes dividing the momentum axis) accessible for a chaotic trajectory. This means that for  $n = 5$  there is, on the average, approximately one rainbow in each box. Thus it is no longer possible to distinguish the rainbows from each other. After  $n = 12$  optical cycles the number of rainbows has exceeded the number of states by a factor of about 1000. This large number of rainbows adds up to a smooth distribution allowing only for small fluctuations as shown in Fig. 5.

More formally, if  $A$  is the phase space area available for the classical motion, at time

$$\frac{t^*}{T} \approx \frac{1}{\lambda} \ln \left( \frac{A}{h} \right) \quad (5)$$

the phase space structure of the classical phase space density evolving from the specified initial distribution (the line  $\{j=0\}$ ) has become so complicated that quantum mechanics cannot resolve the details any longer. This time is referred to by other authors as 'Zaslavsky time' or 'log time' [34], in discussions of semiclassical time-evolution under chaotic dynamics.

Third, there is an exceptional intensity peak, which can still be detected for longer times up to  $n = 24$ . This peak is of a different origin than the rotational rainbows, in particular it does not bifurcate into more and more peaks as time increases. It can, however, accidentally coincide with a rainbow, in which case it is strongly am-

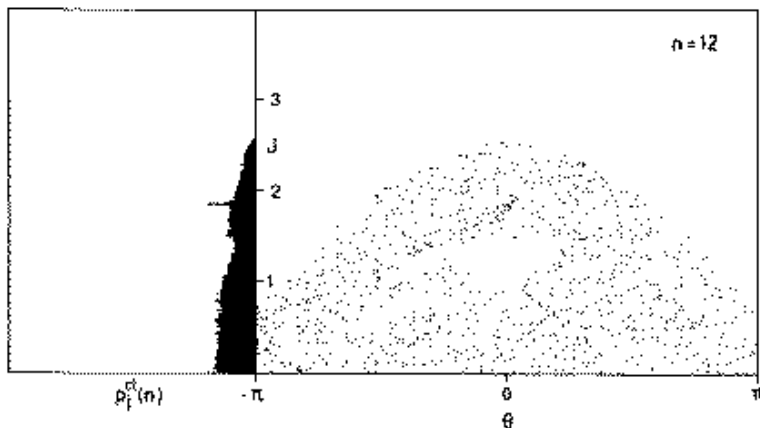


Fig. 5. The Poincaré section of classical phase space for  $t = 12 T$ . On the left the asymptotic classical excitation probability of an initially non-rotating rotor,  $p_j^{cl}(12)$ , is shown as a histogram ( $j = J/h$  with  $h = 0.02$ )

plified. A first hint towards an understanding of this new feature is obtained by closer inspection of the rotational excitation functions  $J(\theta, n)$  shown in Figs. 2 and 3. The density of the points on the curve monitors roughly the intensity along the curve. One observes in all these plots an intensity concentration in a certain region. This can be explained by observing that the above considerations about stretching are not valid for a segment of the curve which is parallel to the so-called stable direction, which can be assigned to any point in the chaotic phase space regime. In almost every point an arbitrary closed curve intersects the stable direction with a nonzero angle. In an exceptional point, however, this angle is zero and the curve describes a parabolic tangent curve in the local coordinate frame of stable and unstable manifolds. For such a point one can find (for each  $n$ ) a neighbourhood on the curve which is not stretched but contracted. This results in an extra peak in the probability distribution at this  $J$ -value. Fixing a length,  $\delta_0$ , a curve segment of size  $\delta_0$  has after  $n$  optical cycles, one obviously sees that, for a segment containing such a special point,  $\delta_0$  decreases exponentially with  $n$  by half (!) of the Lyapunov exponent in contrast to any other segment of the curve. (A detailed analysis includes the curvature of the stable manifold at this particular point as a proportionality factor). Such a special point causes an intensity peak which finally overruns all the rotational rainbows. A clear example is the sharp peak in Fig. 3 for  $n=6$ . It should be noted, that the exceptional points at time  $nT$  are, of course, the iterates of the exceptional points on the initial phase space distribution, i.e. those points where the stable direction is parallel to the line  $J=0$ . There are two such points at  $\theta = 1.95$  and  $\theta = 2\pi - 1.95$ , but only one of the iterates of these points show up in the upper half plane.

### III. Quantum dynamics of a periodically driven 3D rigid rotor

In quantum mechanics the three dimensional time-periodic Hamiltonian in the interaction representation is obtained when the eigenfunctions of the free rotor Hamiltonian,  $Y_{j,m}$ , are used as a basis set. Since the field is directed along the  $z$ -axis (chosen as quantization axis), the  $z$ -component of the angular momentum is conserved and  $m$  is a good quantum number. The results presented here are for  $m=0$ . The Hamiltonian matrix (when the moment of inertia of the molecule is scaled out) is given by

$$H_{j,j'}(t) = \frac{\hbar^2}{2} j(j+1) \delta_{j,j'} + \left( \frac{j}{\sqrt{4j^2-1}} \delta_{j',j-1} + \frac{j'}{\sqrt{4j'^2-1}} \delta_{j',j+1} \right) \times f \cos \omega t. \quad (6)$$

Our analysis is based on quasienergy states, which are discussed in the following section.

#### A. Localized and extended quasienergy states

The time evolution matrix  $\hat{U}(t)$  is obtained by solving the time-dependent matrix problem

$$\hat{H}(t) \hat{U}(\theta|t) = i\hbar \frac{d\hat{U}(\theta|t)}{dt}; \quad t \in [0, T] \quad (7)$$

with the initial condition

$$\hat{U}(\theta|0) = 1. \quad (8)$$

The propagation of  $\hat{U}(\theta|t)$  is carried out by the Adams-Moulton predictor-corrector method [35] using spherical harmonics as a basis set. The quasienergy states [36] are the Floquet solutions of the time-dependent Schrödinger equation

$$\psi_\alpha(\theta, t) = \hat{U}(\theta|t) \psi_\alpha(\theta, 0) \quad (9)$$

such that

$$\psi_\alpha(\theta, t) = e^{-i\omega_\alpha t} \phi_\alpha(\theta, t) \quad (10)$$

where

$$\phi_\alpha(\theta, t) = \phi_\alpha(\theta, t + nT) \quad (11)$$

and  $\epsilon_\alpha = \hbar\omega_\alpha$  are the quasienergies. Note, that in the present case the quasienergy spectrum is pure point as proved recently by Howland [37]. The periodicity  $T = 2\pi/\omega$  is associated with  $\omega$ , the frequency of the monochromatic electromagnetic field. From (9-11) we see that the variational quasienergy states are obtained by calculating the eigenvalues and eigenvectors of the time-evolution matrix  $\hat{U}$  propagated to  $t = T$ ,

$$\hat{U}(\theta|T) \mathbf{C}_\alpha = e^{-i\epsilon_\alpha T} \mathbf{C}_\alpha \quad (12)$$

and

$$\phi_\alpha(\theta, 0) = \sum_j C_{\alpha,j} Y_{j,0}. \quad (13)$$

The quasienergy states are labeled by  $\alpha = 1, 2, \dots$  in increasing order of the corresponding expectation value of  $\hat{H}_0 = \hbar^2 \hat{J}^2/2$ , when  $\hat{J}$  is the (dimensionless) angular momentum operator.

Numerical computations have been carried out using a value of  $\hbar = 0.02$ , which was small enough to demonstrate the quantum-classical correspondence and also numerically tractable (converged results could be obtained expanding in 200 basis functions). As shown in Fig. 6 for there are 96 states (with  $\omega_\alpha T$  values covering almost uniformly the interval  $[0, 2\pi]$ ), which provide almost degenerate states (i.e.  $\langle \alpha | \hat{H}_0 | \alpha \rangle \approx 0.75$ ) as the field is suddenly turned off. Indeed the total classical phase space area inside the chaotic boundary including the regular island inside is 12.06 (compare Fig. 1), which provides exactly  $12.06/\hbar = 96$  ( $\hbar = 2\pi\hbar$ ) states associated with this phase space region as obtained in our quantum calculations.

Moreover, the other quasienergy states,  $\alpha > 96$ , provide expectation values  $\langle \alpha | \hat{H}_0 | \alpha \rangle$ , which are very close

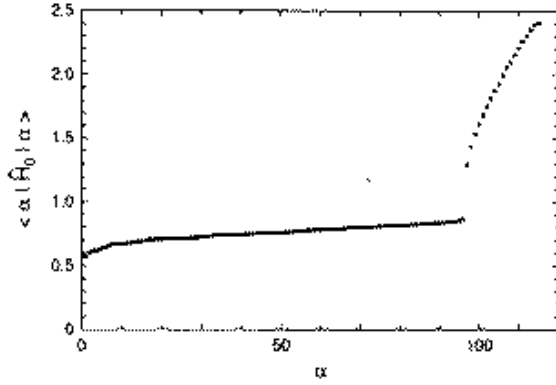


Fig. 6. Expectation values of the field-free Hamiltonian (i.e. the free rotor),  $\langle \alpha | \hat{H}_0 | \alpha \rangle$ , where  $\{|\alpha\rangle\}$  are the quasienergy states

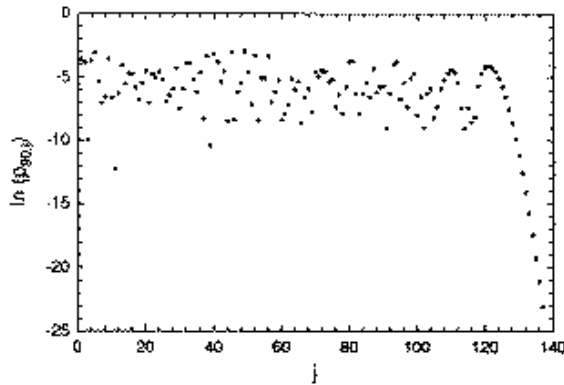


Fig. 7. A characteristic example of an extended quasienergy state ( $\alpha=90$ ) expanded in the basis of the free rotor states. Shown are the projection probabilities  $p_{\alpha,j} = |C_{\alpha,j}|^2$  on a logarithmic scale

to the highly excited energy values of the free rotor and are therefore associated with the outer stability region in the classical phase space as presented in Fig. 1.

The area of the inner stability island is determined as  $0.55 = 4.4 \hbar$ . We would hence expect four or five among the 96 states to be related to the inner stability region. These states should be localized whereas the remaining 91 or 92 should be extended. The absolute squares of the variational coefficients  $C_{\alpha,j}$  defined in (12-13) are the projections of the quasienergy states onto the free-rotor states and give the occupation probabilities of the free-rotor states by the quasienergy states.

$$p_{\alpha,j} = |C_{\alpha,j}|^2, \quad \sum_j p_{\alpha,j} = 1. \quad (14)$$

The  $j$  dependence shows whether a state  $|\alpha\rangle$  is localized or extended in the free rotor energy space. As an example Fig. 7 shows the  $p_{\alpha,j}$  for the quasienergy state  $\alpha=90$ , which is an extended state. One observes a sharp (exponential) decay for  $j > j_m = 130$  due to confinement by the classical KAM-boundary [21, 22]. Free rotor states with  $j < j_m$  are populated with almost equal probability (on a logarithmic scale). This is in agreement with the prediction of 130 populated  $j$ -states obtained classically in Sect. II. These quasienergy states are - in phase space

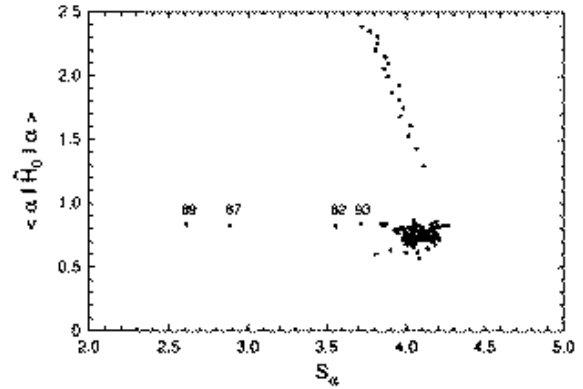


Fig. 8. Expectation value  $\langle \alpha | \hat{H}_0 | \alpha \rangle$  of the field-free Hamiltonian plotted versus entropy  $S_{\alpha}$  for the quasienergy states  $\alpha = 1, \dots, 114$ . Extended states and two classes of localized ones can be distinguished. Some values of  $\alpha$  for low values of the entropy are explicitly specified

- spread over the entire chaotic domain. This will be analysed in detail in Sect. IV.

Several quantities have been introduced for a quantitative description of the statistical distribution of a state with respect to some basis. The first is the number of relevant states, applied first by Haake et al. [38], the second is the mean inverse participation ratio [39]

$$\xi^{-1} = \sum_j p_{\alpha,j}^2. \quad (15)$$

Here we use the Shannon entropy defined as

$$S_{\alpha} = - \sum_j p_{\alpha,j} \ln p_{\alpha,j}, \quad (16)$$

which is a measure of the uncertainty of a state  $|\alpha\rangle$  when only the occupation probabilities  $p_{\alpha,j}$  are known (compare [40]). In Fig. 8 the entropy is plotted versus the value of  $\langle \alpha | \hat{H}_0 | \alpha \rangle$  for the quasienergy states up to  $\alpha=114$ . Such a plot one can be helpful in order to distinguish between extended states and localized ones (this is in the spirit of Fig. 8 in [30] or Fig. 4 in [31]). One observes a 'cloud' of states centered at  $S_{\alpha} = 4.08$  and  $\langle \alpha | \hat{H}_0 | \alpha \rangle = 0.752$ . Above this cloud we observe a clearly separated string of states with entropies decreasing almost linearly with  $\langle \alpha | \hat{H}_0 | \alpha \rangle$ . These are the states  $\alpha \geq 96$  associated with the outer stability region, which are in phase space supported by invariant curves allowing only for the population of a confined number of free rotor states. This number of states depends on the shape of the invariant curves and decreases to unity in the limit  $\alpha \rightarrow \infty$ .

A second string of states appears for an almost constant value of  $\langle \alpha | \hat{H}_0 | \alpha \rangle = 0.83$ , which agrees with the classical value of  $H_0$  for the stable fixed point in the center of the inner stability island. We can hence assign these four states to the inner stability region. The remaining 92 quasienergy states belonging to the 'cloud' can be related to the chaotic classical phase space region. A quantum estimate for the number of states captured by a resonance is given in [32].

In Fig. 9 the quantum mechanical rotational probability

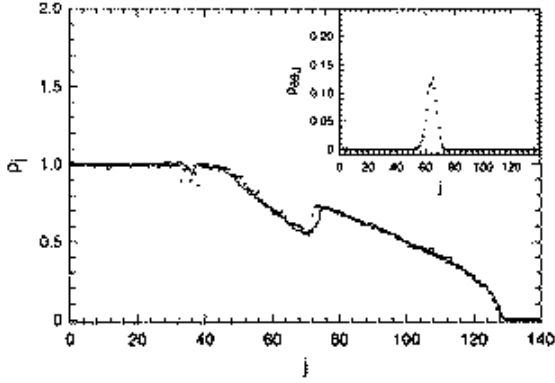


Fig. 9. Quantum mechanical densities projected onto the free-rotor states summed over the 92 extended states (●) in comparison with the classical density obtained by projecting the chaotic phase space (histogram). The inset shows as a typical example of a localized quantum state the projection onto the free-rotor basis for the state with lowest entropy ( $\alpha = 89$ )

$$\rho_j^{qm} = \sum_{\alpha} p_{\alpha,j} \leq 1, \quad (17)$$

where the prime indicates that the sum runs over all  $N = 92$  chaotic quasienergy states (note, that  $\rho_j^{qm}$  satisfies  $\sum \rho_j^{qm} = N = 92$ ). The agreement with the discrete classical density is quite remarkable. The contribution of the state with the lowest entropy in the insert of Fig. 9 shows very clear the localization of this state.

### B. Rotational momentum transfer

In order to study the probability to transfer angular momentum to the rigid rotor (which describes the 3D rotational motion of a diatomic molecule) we should calculate the time-dependent solution of the Schrödinger equation,  $\Phi(\theta, t)$ , with the initial condition of  $\Phi(\theta, 0) = \sqrt{1/2\pi}$ , which implies that the rotor (diatom) is in its rotational ground state as the field is suddenly turned on. The probability to excite the initially non-rotating diatomic molecule to rotational state  $j$  resulting from the interaction with the electromagnetic field after  $n$  optical cycles (i.e.  $t = nT$ ) is given by

$$p_j(n) = |\langle \Phi(t = nT) | Y_{j,0} \rangle|^2. \quad (18)$$

If  $|\Phi(t = nT)\rangle$  is expanded in terms of the quasienergy basis functions one immediately gets

$$p_j(n) = \left| \sum_{\alpha} C_{\alpha,j}^* C_{\alpha,0} \exp(-in\omega_{\alpha} T) \right|^2, \quad (19)$$

where  $\exp(-i\omega_{\alpha} T)$  and  $C_{\alpha}$  are, correspondingly, the eigenvalues and eigenvectors of  $\hat{U}(0|T)$  (see (12)).

The results presented in Figs. 10–15 clearly show that there is *no* quantum limitation to the classical dynamics. We can, however, not exclude that there could be dynamical localization in different parameter regimes (larger value of  $\hbar$ , larger amplitude of the driving force). In this case the absence of localization for our choice of parameters would be a consequence of the fact that the locali-

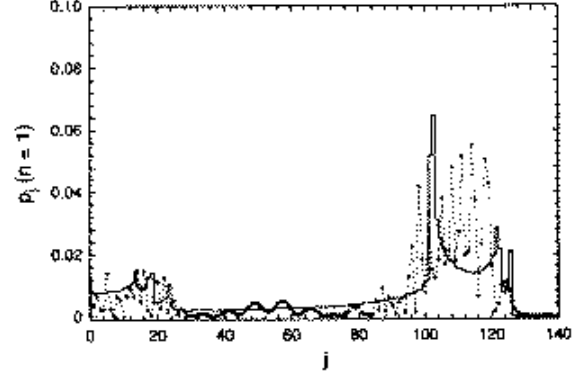


Fig. 10. The probability  $p_j(n)$  (●) to excite the non-rotating rotor to its  $j^{\text{th}}$  rotational excited state after *one* optical cycle ( $n = 1$ ), when  $\hbar = 0.02$ . The histogram gives the classical result

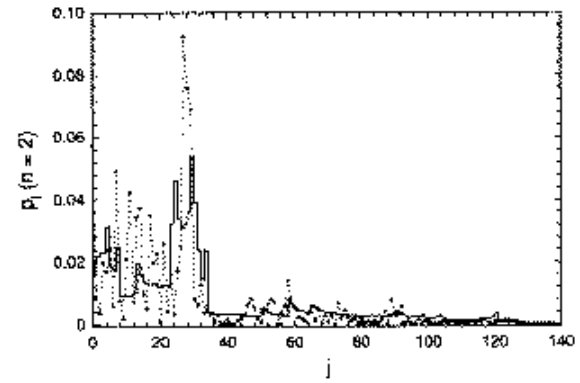


Fig. 11. The quantum probability  $p_j(n)$  (●) to excite the non-rotating rotor to its  $j^{\text{th}}$  rotational excited state after *two* optical cycles ( $n = 2$ ), when  $\hbar = 0.02$ . The histogram gives the classical result

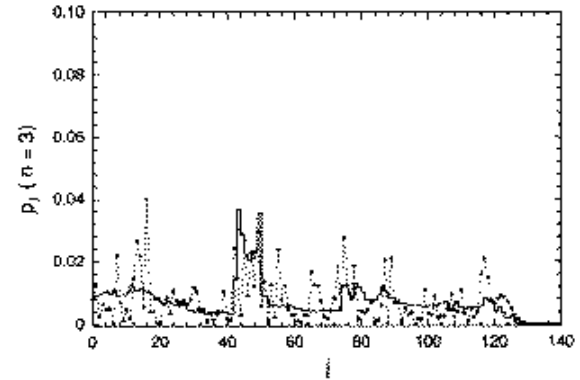


Fig. 12. The quantum probability  $p_j(n)$  (●) to excite the non-rotating rotor to its  $j^{\text{th}}$  rotational excited state after *three* optical cycles ( $n = 3$ ), when  $\hbar = 0.02$ . The histogram gives the classical result

zation length is larger than the limitation due to KAM-borders. Recently, Graham and Keymer and Graham et al. [29] detected and analysed this phenomenon in a Josephson junction model. Such an investigation for our model, however, is beyond the scope of this paper and would be a study for itself.

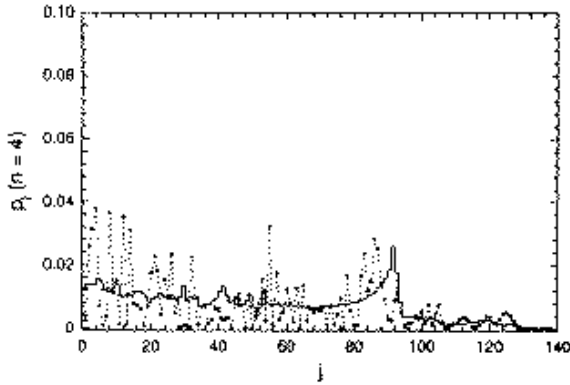


Fig. 13. The quantum probability  $p_j(n)$  ( $\bullet$ ) to excite the non-rotating rotor to its  $j^{\text{th}}$  rotational excited state after *four* optical cycles ( $n=4$ ), when  $\hbar=0.02$ . The histogram gives the classical result

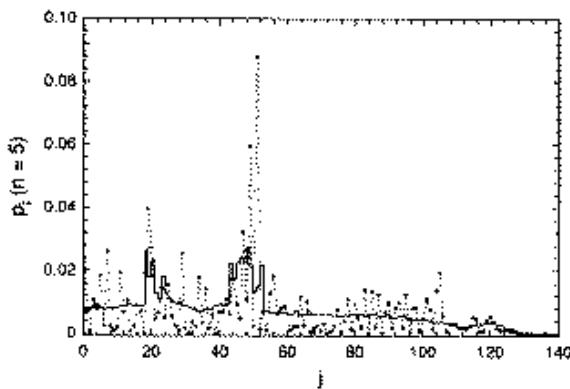


Fig. 14. The quantum probability  $p_j(n)$  ( $\bullet$ ) to excite the non-rotating rotor to its  $j^{\text{th}}$  rotational excited state after *five* optical cycles ( $n=5$ ), when  $\hbar=0.02$ . The histogram gives the classical result

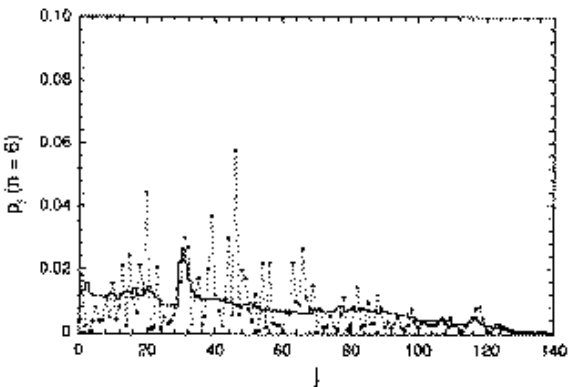


Fig. 15. The quantum probability  $p_j(n)$  ( $\bullet$ ) to excite the non-rotating rotor to its  $j^{\text{th}}$  rotational excited state after *six* optical cycles ( $n=6$ ), when  $\hbar=0.02$ . The histogram gives the classical result

During the first periods the quantum  $j$  distribution shows the rotational rainbow structures which were obtained in the classical calculations discussed above. The fact that there are two rainbow structures and the suppression of rotational excitation in the region  $45 \leq j \leq 75$  can be related to the existence of the inner regular island

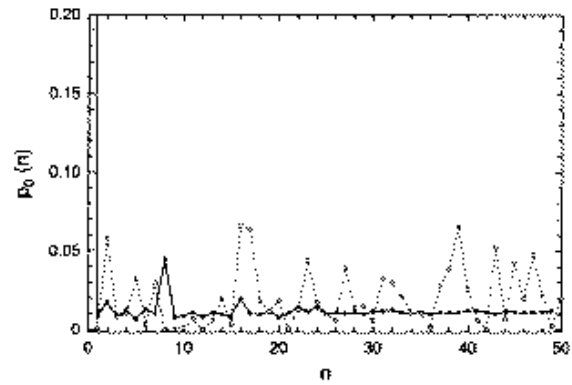


Fig. 16. Survival probability  $p_0(n)$  ( $-O-$ ) as function of the number  $n$  of optical cycles (i.e. at time  $t=2\pi n$ ) when  $\hbar=0.02$ . Also shown are the classical results ( $-O-$ )

embedded in the chaotic sea. In addition to the main rainbow maxima the quantum distributions also show characteristic secondary maxima and minima, known as rotational rainbow oscillations, which can be interpreted semiclassically by constructive or destructive interference of a small number of contributing classical paths [33].

After about three optical cycles (see Figs. 12-15) the clear classical and quantum correspondence disappears and the distributions are apparently different, which results from a pure phase interference effect due to the proliferation of the number of interfering classical paths which increases exponentially as discussed in Sect. II. The only exception are the extraordinary rainbows described in Sect. II. Due to their dominance they cause also high quantummechanical excitation probabilities which can be distinguished from fluctuations up to times  $n=6$ . For larger times the quantum probabilities are dominated by strong fluctuations resulting from almost random phase interferences as analyzed in more detail in Sect. IV.

Finally, the quantum vs. classical results presented in Fig. 16 clearly show that the probability to find the diatom in the ground rotational state  $j=0$  is on the average about 2.5% and always less than 25% during the first 50 periods, which is much larger than the value of about 1% obtained classically. This will be analysed in more detail in the following section.

A 3D plot of the  $p_j(n)$  obtained from numerical calculations for  $\hbar=0.02$  is presented in Figs. 17-18 as a function of  $j$  and  $n$ . First one can see that the rotational rainbow structures obtained after one optical cycle disappear rapidly as time increases and all rotational states from  $j=0$  to  $j=130$  are populated. The confinement of the occupation probabilities of the angular momentum states of the rotor to  $0 \leq j \leq 130$  can be clearly seen also from the surface of section at  $p_j = 1/92$  represented in Fig. 19, where the dark area denotes occupation probabilities of  $j$  where  $p_j > 1/92$  and the white area where  $p_j \leq 1/92$ . The density of the dark area is almost constant for  $j < 50$  which is an excellent agreement with the classical results (see Figs. 1 and 4), which show an equal probability  $\overline{p_j} = 1/92$  to find the rotor at  $J < 0.9$  (i.e.  $j \leq 45$  for  $\hbar=0.02$ ) and gradually reduces to zero as  $j \rightarrow 130$  (i.e.  $J = 2.6$  for  $\hbar=0.02$  as shown in Fig. 1).

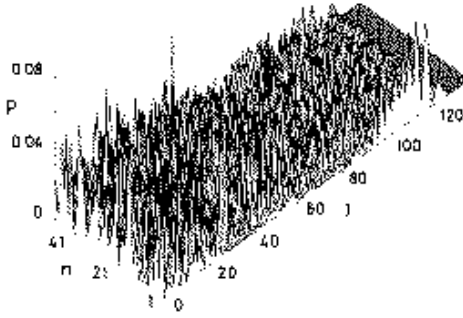


Fig. 17. 3D representation of the quantum excitation probability,  $p_j(n)$ , of the angular momentum  $j$  at time  $t=nT$  when  $T=2\pi$  is the periodicity of the field ( $\hbar=0.02$ ). At  $t=0$  (not shown in the plot)  $p_j(0)=\delta_{j,0}$ . A number of 130 states are strongly populated

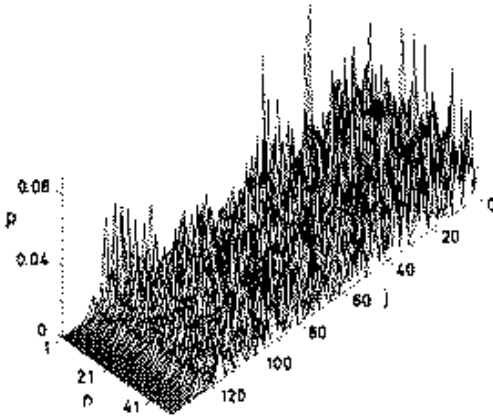


Fig. 18. Same as Fig. 17, however seen from the opposite direction demonstrating the smooth decay to zero for  $N > 130$

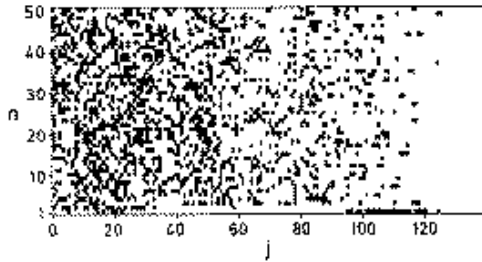


Fig. 19. Surface of section of  $p_j(n)$  shown in Figs. 17 and 18. Regions of strong excitation ( $p_j(n) \geq 1/92$ ) are colored black

The visual impression from Figs. 17–19 is a surprising degree of randomness in the behavior of  $p_j(n)$ , which reminds one very much of grass growing erratically in a meadow. The basic idea is that any pure state (here the state  $|j=0\rangle$ ) will become a random state under the unitary time evolution after a time of the order of the log time, whose fluctuations can be described purely statistically as discussed in the next section in detail. It should finally be noted that the numerical results presented here have been obtained for a time scale shorter than the so

called ‘Heisenberg time’ or ‘break time’  $2\pi\hbar/\overline{\Delta\varepsilon}$ , where  $\overline{\Delta\varepsilon} = \hbar\Delta\omega/T$  is a typical level spacing, yielding a break time of about  $NT$  in the present case.

#### IV. Statistics of eigenvector components and intensity fluctuations

During the last two decades several ways were found in which classical chaotic dynamics manifests itself in quantum dynamics, the most prominent among them being the level statistics of classical chaotic systems predicted on the basis of random matrix theory (see [2]). In order to understand more about ‘local’ features of the quantum analog of chaotic systems an approach was made to analyse statistics of eigenvector components. Especially in the case of systems, which are not entirely chaotic and where chaos shows up in layers coexisting with regular motion, this seems to be more useful than analysing the spectrum as a whole. The basic idea behind this approach is to regard the eigenvectors as random unit vectors in an  $N$ -dimensional vector space, where  $N$  is determined by the underlying classical dynamic and the value of  $\hbar$ . The basic theory of random vectors can be found in [42, 43, 41, 40, 44, 45]. In the following a brief outline of the theory is given and the statistical properties of both the squares of the expansion coefficients  $C_{x,j}$  and the quantum rotational excitation probabilities  $p_j(n)$  for the driven rotor are analysed in more detail.

Suppose we have a  $d$ -dimensional real vector space and a normalized vector  $|\psi\rangle$  is chosen at random with respect to the uniform distribution over the unit sphere in this space. The basic quantities of interest are the statistical distributions of the expectation value  $p$  of a projection of  $|\psi\rangle$  onto a  $v$ -dimensional subspace. This is the basis for studying fluctuations in vector components and expectation values of observables. The distributions can be obtained by elementary integration (see e.g. Zimmermann et al. [41]) yielding

$$P_v(p) = \frac{\Gamma(d/2)}{\Gamma(v/2)\Gamma((d-v)/2)} p^{v/2-1} (1-p)^{d-v/2-1}, \quad (20)$$

where mean and variance are given by

$$\bar{p} = \frac{v}{d}, \quad (\Delta p)^2 = \frac{2v(d-v)}{d^2(d+2)}. \quad (21)$$

In the limit of large  $d$  and small ratio  $\hat{p} = v/d$  the  $P_v(p)$  in (20) approaches a  $\chi_v^2$  distribution:

$$P_v(p) \approx \chi_v^2(p) = \left(\frac{v}{2\hat{p}}\right)^{v/2} \frac{1}{\Gamma(v/2)} p^{(v/2)-1} \exp\left(-\frac{vp}{2\hat{p}}\right). \quad (22)$$

The  $\chi_v^2$  distribution describes the statistics of a sum of  $v$  absolute squares of independent Gaussian variables. Thus, approximating the rigorous distribution (20) by the  $\chi_v^2$  distribution means neglecting correlations between vector components due to the constraint of unit length. This is justified in the limit  $d \rightarrow \infty$  (see e.g. the discussion by

Wooters [40]). The  $\chi_\nu^2$  distribution can also be derived directly using the maximum entropy principle [43]. For the case of  $\chi_\nu^2$  distributions the relation

$$\overline{p^2} = \left( \frac{2}{\nu} + 1 \right) \overline{p}^2 \quad (23)$$

is valid yielding a variance of

$$(\Delta p)^2 = \frac{2}{\nu} \overline{p}^2 = \frac{2\nu}{d^2} \quad (24)$$

This variance is larger than for the correct distribution (20), but with the relative difference to (21) is of order  $\nu/d$  and hence vanishes in the limit  $d \rightarrow \infty$ .

For the system under investigation here, we have to assume that the Hilbert space can be separated into a 'chaotic' one of dimension  $N$ , spanned by extended Floquet states associated with the chaotic regime, and a regular one spanned by the localized states. In the preceding section we have shown that this separation works quite well yielding a dimension of  $N=92$ , which is determined by the size of the chaotic phase space. Within this 'chaotic' subspace the system may be described by an circular ensemble of random matrices. The symmetry class of the system determines whether the orthogonal, unitary, or symplectic ensemble should be applied and hence which of the  $\chi_\nu^2$  distributions describes the statistics of the eigenvector components correctly [2, 40, 44, 46].

In our case we have a system with time reversal symmetry, hence the Floquet states form an orthogonal set and their components should follow the  $\chi_\nu^2$  distribution with  $d=N$ ,  $\nu=1$

$$\chi_1^2(p) = \frac{1}{\sqrt{2\pi p N}} e^{-pN/2}, \quad (25)$$

which is known as Thomas-Porter distribution. The time evolution, however, is to be described by an unitary ensemble such that components of a time propagated state should follow the  $\chi_\nu^2$  distribution with  $d=2N$ ,  $\nu=2$  being simply the exponential distribution

$$\chi_2^2(p) = N e^{-pN}. \quad (26)$$

In this case vector components are regarded as complex numbers, whose real and imaginary part are independent random Gaussian variables.

In the following we will check these statistical predictions for two quantities of interest: First, the weight coefficients  $p_{s,j} = |C_{s,j}|^2$  of individual quasienergy states in the free rotor basis (14) as a test case for  $\chi_1^2$ , and, second, the dynamical time evolution of a state vector in terms of the excitation probability  $p_j(n)$  of rotational state  $j$  after  $n$  optical cycles (18) as a test case for  $\chi_2^2$ . Before doing so, we refer to some very useful results for the entropy. As Jones [45] has shown, the distribution (20) allows for an analytical evaluation of the integral

$$s_\nu = - \int_0^\infty p \ln p P_\nu dp, \quad (27)$$

which is the mean value of  $-p \ln p$  with respect to the  $P_\nu$  distribution. The entropy (16) of a random vector with  $N$  components (i.e. the entropy averaged over all vectors on the unit sphere in the  $N$ -dimensional vector space) is hence  $S_\nu = N s_\nu$ . The results is

$$S_\nu = \Psi(\nu N/2 + 1) - \Psi(\nu/2 + 1), \quad (28)$$

where  $\Psi$  is the digamma function. Życzkowski [44] and Wooters [40] obtained approximations by replacing the exact distribution  $P_\nu$  in (27) by the  $\chi_\nu^2$  distribution (26) yielding

$$S_\nu = \ln N + (\ln \nu/2 - \Psi(\nu/2 + 1)), \quad (29)$$

valid in the limiting case of large  $N$ . For the two particular cases considered above the results are [40]:

$$\begin{aligned} S_1 &= N s_1 = \ln N - (2 - \ln 2 - c) \\ &= \ln N - 0.729637\dots \end{aligned} \quad (30)$$

$$S_2 = N s_2 = \ln N - (1 - c) = \ln N - 0.422784\dots, \quad (31)$$

where  $c$  is Euler's constant, i.e. the entropy of a random vector with  $N$  components is the maximum available entropy,  $\ln N$ , lowered by a constant not depending on  $N$  but only on the type of the  $\chi_\nu^2$  distribution.

Applying these results to the weight coefficients  $p_{s,j}$  of the 92 extended Floquet states found for the driven rotor as specified in Sect. III one has to take into consideration that the free-rotor basis (13) is overcomplete on the vectorspace of the  $N=92$  extended Floquet states. The projection  $\rho_j^{qm}$  (17) of a state  $|j\rangle$  is smaller than unity depending on the value of  $j$ . Consequently, the mean value of the coefficients  $p_{s,j}$  is  $j$ -dependent:

$$\overline{p}_j = \frac{1}{N} \sum_s p_{s,j} = \frac{\rho_j^{qm}}{N} \leq \frac{1}{N}. \quad (32)$$

Here and in the following the prime indicates that the sum only runs over the 92 extended quasienergy states. When the coefficients can be considered as independent random variables, a generalization to this case is straightforward by replacing  $1/N$  in (25) by the individual mean values  $\overline{p}_j$  leading to different distributions for any particular values of  $j$ :

$$P_j(p_j) = \frac{1}{\sqrt{2\pi p \overline{p}_j}} e^{-p_j/2\overline{p}_j} \quad (33)$$

and

$$(\Delta p_j)^2 = 2 p_j^2 = 2 (\rho_j^{qm}/N)^2. \quad (34)$$

In our case the expansion coefficients for  $j \leq 47$  can be expected to follow the same statistics, since they have almost the same mean value (compare the discussion of the results shown in Fig. 9). The resulting statistics of the coefficients is presented in Fig. 20 in a convenient plot of  $P(\ln p) = \sqrt{p/2\pi \overline{p}} e^{-p/2\overline{p}}$  versus  $p$  [43] because of the singular character of the Thomas-Porter distribution. In such a plot the distribution shows a global maximum at  $-\ln N$  with a width depending on the type  $\nu$  of the dis-

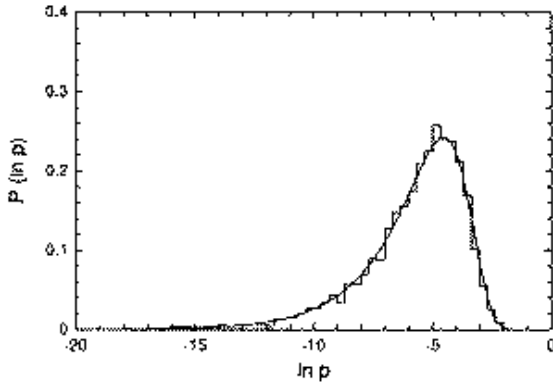


Fig. 20. Statistics of the projection probabilities  $p_{\alpha,j} = |C_{\alpha,j}|^2$  of the extended quasienergy states on the free rotor basis for  $j \leq 47$ . The probability density for finding a value of  $\ln p_{\alpha,j}$  is shown as a histogram together with the predicted Thomas-Porter curve

tribution. Note, that such a plot directly describes the visual impression from Fig. 7, where the maximum of the distribution appears as a plateau. The obtained histogram is in very good agreement with the predicted  $\chi^2$  curve, in particular in regard of the relatively small number of data. Even more impressive is the comparison of the relative variance  $(\Delta p)^2/\bar{p}^2 = 1.9935$  obtained from the data with the predicted value of 2 from (34).

In the preceding chapter we have already plotted the entropy of the Floquet states (see Fig. 8). The mean value of the entropy over the extended states

$$\bar{S} = \frac{1}{N} \sum_{\alpha} S_{\alpha} = -\frac{1}{N} \sum_{\alpha} \sum_j p_{\alpha,j} \ln p_{\alpha,j} \quad (35)$$

can be approximated by replacing the  $\alpha$  summation by an integral over the distribution (33):

$$\begin{aligned} \bar{S} &= -\sum_j \int p_j \ln p_j P_j(p_j) dp_j \\ &= -\sum_j \frac{\rho_j^{qm}}{N} \left( \ln \left( \frac{\rho_j^{qm}}{N} \right) + (1-c) \right) \\ &= -\sum_j \bar{p}_j \ln \bar{p}_j - (1-c) \\ &= S(\bar{p}_0, \bar{p}_1, \dots) - (1-c). \end{aligned} \quad (36)$$

Here we have again substituted  $1/N$  in (31) by  $\bar{p}_j$ . This result nicely connects the mean value of the entropy with the entropy of the mean probability  $\bar{p} = \rho^{qm}/N$ , which is of course larger. Since in our case the mean density  $\rho^{qm}$  agrees with the discrete projection  $\rho^{cl}$  of the classical phase space density, the entropy  $S(\bar{p}_0, \bar{p}_1, \dots)$  of the mean probability can be calculated fully classically. In this way (36) separates the entropy in a value determined by the classical phase space projection and a constant due to the fluctuations. Note that in the limit  $\hbar \rightarrow 0$  the entropy grows asymptotically as  $\ln \hbar$  making the constant difference  $1-c$  negligible. Due to Wooters [40] it is possible to find an analytical formula for the mean deviation of the entropy from the mean value  $\bar{S}$  only in the case  $\nu = 2$ . However, in any case the mean relative fluctuation will depend on

$N$  as  $1/\sqrt{N}$  thus going to zero like  $\sqrt{\hbar}$  in the classical limit  $\hbar \rightarrow 0$ . In our example we obtained for the mean of the entropies of the 92 extended states a numerical value of  $\bar{S} = 4.0686$  and for the entropy of the mean density  $S(\bar{p}_0, \bar{p}_1, \dots) = 4.7816$  yielding a difference of 0.713 which is in quite good agreement with the predicted value of  $1-c = 0.729\dots$  The classical counterpart of  $S(\bar{p}_0, \bar{p}_1, \dots) = 4.7816$  obtained from the discrete classical phase space projections  $\rho_j^{cl}$  yields a value of 4.776 (compare again Fig. 9) in good agreement with  $S(\bar{p}_0, \bar{p}_1, \dots)$  as expected.

Rather than evaluating the statistics of vector components, fluctuations in matrix elements of operators have been analysed (see, e.g., [46]). It is stated that the relative fluctuations of such matrix elements should also be described by a  $\chi^2$  distribution. Here we will confine ourselves to a brief analysis of the expectation values of the field free Hamiltonian in the extended Floquet states in order to explain the effect of quasi degeneration observed in Sect. II.

Starting from the fluctuations of vector components one is able to derive results for the mean and the fluctuation of expectation values of hermitian operators not commuting with the quasienergy operator. Suppose our overcomplete basis  $\{|j\rangle, j=1, \dots, M \geq N\}$  is chosen as the eigenbasis of an hermitian operator  $\hat{B}$ :

$$\hat{B}|j\rangle = b_j|j\rangle, \quad j=1, \dots, M. \quad (37)$$

The expectation value of  $\hat{B}$  for a state  $|\psi\rangle$  is then given by

$$B = \langle \psi, \hat{B} \psi \rangle = \sum_{j=1}^M \langle \psi, \hat{\Pi}_j \psi \rangle b_j = \sum_{j=1}^M p_j b_j, \quad (38)$$

where  $\hat{\Pi}_j$  denotes the projection onto the state  $|j\rangle$  and  $p_j$  its expectation value. Averaging over all unit vectors in the  $N$  dimensional vector space using (32) shows that the mean is simply the average over the eigenvalues weighted by the projection of the corresponding eigenvector onto the  $N$ -dimensional subspace:

$$\bar{B} = \sum_{j=1}^M \bar{p}_j b_j = \frac{1}{N} \sum_{j=1}^M \rho_j^{qm} b_j. \quad (39)$$

Furthermore, using relation (24) for the variance of the  $\chi^2$  distribution, a short calculation yields for the variance of the expectation value

$$(\Delta B)^2 = \frac{2}{\nu} \sum_{j=1}^M (\bar{p}_j b_j)^2 = \frac{2}{\nu N^2} \sum_{j=1}^M (\rho_j^{qm} b_j)^2, \quad (40)$$

if  $p_j$  is distributed according to a  $\chi^2$  distribution. (40) was derived assuming independent fluctuations in the individual  $p_j$ . The correlations between them, though they are small, will in any case reduce the fluctuations in the expectation values. Hence, (40) provides only an upper estimate for the fluctuation of the expectation values. Interestingly, (39) has a classical analog, namely the mean of the classical analog of  $\hat{B}$  over the microcanonical ensemble, i.e. the average with respect to the classical invariant density [47]. There is no classical analog of (40).

However, it is just a general form of the well known statistical result, that the fluctuations of an average over  $N$  independent variables is reduced by a factor of  $1/\sqrt{N}$  compared with the fluctuations of the single variables.

One expects that an operator  $\hat{B}$  will provide almost the same expectation value for any state, which is extended in the eigenbasis of  $\hat{B}$ , with decreasing fluctuations if the dimension  $N$  is increased. Semiclassically, the dimensions  $N$  and  $j_m$  scale inversely with  $\hbar$ . Thus, in the limit  $\hbar \rightarrow 0$  the number of contributions to the sum in (40) increases as  $1/\hbar$ , with the single contributions converging to the classical value. This implies, that the variance decreases as  $\Delta B \sim \sqrt{\hbar}$ . In the classical limit,  $\hbar = 0$ , complete degeneration is achieved.

In our example the hermitian operator can be taken as the free rotor Hamiltonian  $\hat{H}_0$ . In Fig. 6 the expectation values of  $\hat{H}_0$  for the Floquet states are shown for  $\hbar = 0.02$ . The results from (39) and (40) are  $\bar{H}_0 = 0.752$  and  $\Delta \langle H_0 \rangle = 0.112$ . With exception of the state  $\alpha = 1$  all states up to  $\alpha = 96$  lie in a strip defined by these two values. In particular the mean value of the 92 extended quasienergy states agrees precisely with  $\bar{H}_0$  and also with the classical average over the chaotic area. The predicted value of the mean deviation, however, is almost a factor of 2 too large, the mean deviation of the 92 expectation values of  $\langle H_0 \rangle$  is actually only 0.60. As already anticipated above, this deviation is due to the neglected correlations between the individual fluctuations in (40).

In the following we evaluate the rotational excitation probabilities shown in Figs. 17–19 in more detail.

A closer analysis of these excitation probabilities starts with separating them into their mean value and the fluctuation. (19) allows for determining the long time average of the excitation probabilities from the expansion coefficients:

$$\begin{aligned} p_j^\infty &= \lim_{n \rightarrow \infty} \frac{1}{n} \sum_{k=0}^n p_j(k) \\ &= \sum_{\alpha} |C_{\alpha,j}^* C_{\alpha 0}|^2 = \sum_{\alpha} p_{\alpha,j} p_{\alpha,0}. \end{aligned} \quad (41)$$

Since the initial state is almost entirely located in the space spanned by the  $N = 92$  extended states we expect this sum to have  $N$  relevant contributions. The value of this sum can be roughly estimated by replacing  $p_{\alpha,0}$  by its mean value  $1/N$  and recalling relation (23) for the  $\chi^2$ -distribution. We obtain

$$\bar{p}_j^\infty \approx \begin{cases} p_j = \frac{1}{N} \rho_j^{qm} & j \neq 0 \\ \bar{p}_0 = \frac{3}{N} \rho_0^{qm} & j = 0 \end{cases} \quad (42)$$

and, since the quantum densities  $\rho_j^{qm}$  agree with the discrete classical phase space projections  $\rho_j^{cl}$ , we expect, at least in the limit  $\hbar \rightarrow 0$ , the quantum excitation probabilities to be close to the normalized discrete classical densities, i.e. the averaged classical excitation probabilities  $p_j(\infty) = \rho_j^{cl}/N$ . They should hence be almost constant

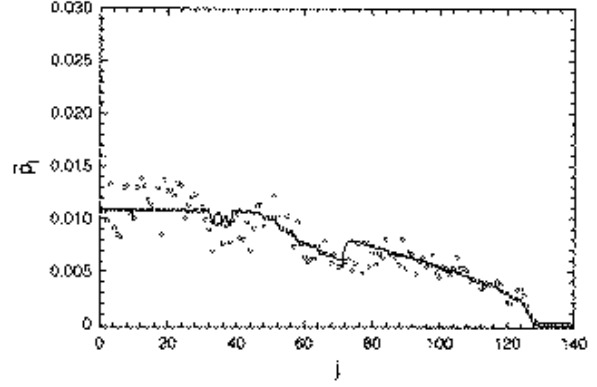


Fig. 21. Mean excitation probability  $\bar{p}_j^\infty$  (—○—) compared with the normalized quantum density  $\rho_j^{qm}/N$  (—●—)

for  $j \leq 47$  (see again Fig. 9), which agrees with the rough optical impression one can get from Fig. 19. Remarkable is that the average survival probability  $\bar{p}_0^\infty$  is expected to be three times larger than the others with a comparable density  $\rho_j^{qm}$ . This factor of three is due to the fact that the  $C_{\alpha,j} = \langle \alpha | j \rangle$  satisfy the statistics of an orthogonal vector ensemble as well as the coefficients of the initial state  $|\psi(t=0)\rangle = |j=0\rangle = \sum_{\alpha} C_{\alpha,j} |\alpha\rangle$ . For more general cases the expansion coefficients are chosen from a unitary vector ensemble leading to a factor of two instead of three [42].

The long time average excitation probabilities  $p_j^\infty$  plotted in Fig. 21 show a considerable oscillatory structure agreeing on the average with the normalized classical density  $\rho_j^{qm}/N$ . The value for the survival probability is found to be  $\bar{p}_0^\infty = 2.15/92$ .

The impression from Figs. 17–18 is that the excitation probabilities  $p_j(n)$  fluctuate almost randomly at least for times larger than the log-time. Due to the unitarity of the time evolution these fluctuations should follow the  $\chi^2$ -distribution (22):

$$P_j(p_j) = \frac{1}{\bar{p}_j} e^{-p_j/\bar{p}_j}. \quad (43)$$

In Fig. 22 the probability distribution for finding a rotational excitation probability  $p$  for the combined distributions  $p_j(n)$ ,  $j = 1, \dots, 47$  and  $n = 6, \dots, 50$  is shown on a logarithmic scale, i.e. only times larger than the log-time are considered. Though the mean values  $\bar{p}_j$  are not equal as shown in Fig. 21, one nevertheless observes an overall exponential decay  $P_j(p_j) \approx \bar{p}^{-1} e^{-p/\bar{p}}$  with slope  $1/\bar{p} \approx 92$  in agreement with the number of extended states.

These findings show that the deterministic time propagation can be considered as practically random for times exceeding the log-time. This is remarkable, in particular because the predicted statistics is valid when averaging over all unit vectors of the underlying complex vector space, which is actually a  $N$ -dimensional complex space. When propagating one vector in time, however, only  $N$  real parameters (the phases) are varied, whereas the absolute values of the vector components in the quasienergy basis are fixed forever.

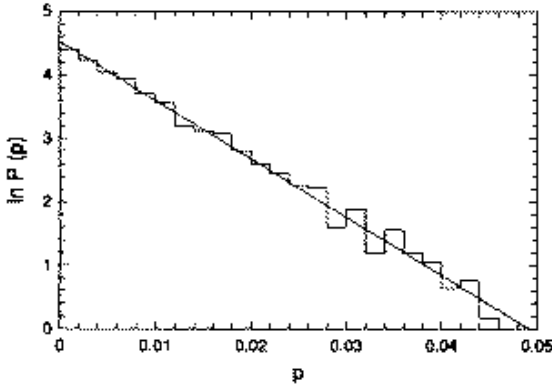


Fig. 22. Statistics of the rotational excitation probabilities  $p_j(n)$  shown in Figs. 17–19. The probability density for finding a value of  $p_j(n) = p$  is shown as a histogram on logarithmic scale. Only data  $1 \leq j \leq 47$  and  $6 \leq n \leq 50$  are taken into account. Also shown is the predicted exponential decay (i.e. a straight line) with slope  $N=92$

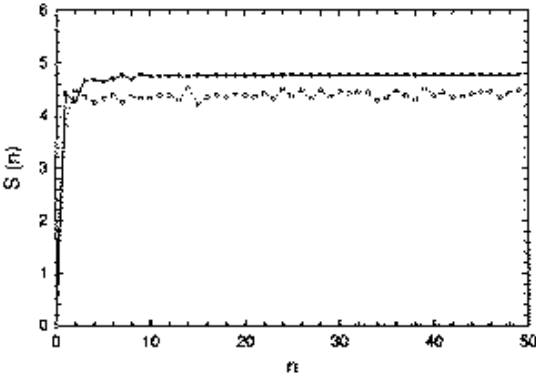


Fig. 23. Time dependence of the entropy  $S(n)$  (—○—) defined in (16) as function of the time  $t = 2\pi n$ , where  $2\pi$  is the periodicity of the field ( $\hbar = 0.02$ ). Also shown is the classical entropy (—●—) calculated from the classical probabilities (histograms)

Finally, in Fig. 23 we show the entropy

$$S(n) = - \sum_j p_j(n) \ln p_j(n). \quad (44)$$

of the time propagated state as a function of time. Starting from zero, the entropy rapidly increases and oscillates with an average value of  $\bar{S} = 4.386$  for  $n \geq 3$ . Also shown is the classical entropy  $S_c(n)$  of the classical excitation probabilities  $p_j(n)$  which converges to a value of  $S_c^\infty = 4.776$  in the long time.

Again, this can be understood within this approach of random vector theory. As for the entropy of the quasienergy states discussed above, one can again relate the long time average of the entropy

$$\bar{S}^\infty = \lim_{n \rightarrow \infty} \frac{1}{n} \sum_{k=1}^n S(k) \quad (45)$$

to the entropy of the mean probabilities

$$S(\bar{p}_0^\infty, \bar{p}_1^\infty, \dots) = - \sum_j \bar{p}_j^\infty \ln \bar{p}_j^\infty. \quad (46)$$

Since in this case the fluctuations follow a  $\chi^2$  distribution one expects from (36) a difference of

$$S(\bar{p}_0^\infty, \bar{p}_1^\infty, \dots) - \bar{S}^\infty = 0.4112\dots \quad (47)$$

As already anticipated in the discussion of the entropy of the quasienergy states, this formula expresses the expectation value of the entropy in a term which allows for a classical computation which scales like  $\ln \hbar$  and a constant difference due to the fluctuations which is negligible in the classical limit. In the example studied here, the entropy of the average probabilities was found numerically to be  $S(\bar{p}_0^\infty, \bar{p}_1^\infty, \dots) = 4.759$ , which compares well with the value of 4.756 calculated from the normalized quantum density  $\rho^{qm}/N$  as well as the classical limit  $S_c^\infty = S(\rho_1^c, \rho_2^c, \dots) = 4.776$ . The long time limit calculated as an average of the  $S(n)$  for  $n=6\dots 50$  yields  $\bar{S}^\infty \approx 4.38$ , which is 0.38 smaller than the  $\bar{S}$  again in good agreement with (47).

## V. Concluding remarks

We presented a detailed quantitative analysis of the quasienergy states and the rotational excitation dynamics in a continuously driven rotor system. The fact that 92 extended quasienergy states were obtained, exactly as predicted on the basis of the classical calculations, and all of them provide about the same probability (on logarithmic scale) to excite the free rotor to  $j \leq 130$  (again as predicted from the classical calculations) show that there is no strong quantum limitation of classical chaos. As a consequence, the quantum evolution follows the classical evolution revealing rotational rainbow structures in the spectrum for the first optical cycles, which are rapidly quenched in time. For times larger than a characteristic time  $t^*$  the rotational spectrum allows for a purely statistical description.

Both the expansion coefficients of the quasienergy states in the free-rotor basis and the rotational excitation probabilities can be understood as projections of random vectors whose mean values are determined by the classical phase space. The fluctuations of these coefficients are in remarkable agreement with statistical predictions of random vector theory. In particular it was demonstrated that the time evolution generates a random vector. Related examples of systems where pure states behave like random vectors are rare. Notable examples are the kicked top studied by Haake et al. [38] (see also the extensive discussion in [2]) and the related perturbed dynamics [48]. For the driven rotor studied here the randomness appears to be most clearly observable.

Further studies are, however, indicated, in particular realistic systems, which allow experimental investigations. This seems to be possible for the driven rotor.

As proposed by Blümel, Fishman and Smilansky [23] diatomic molecules with large rotational constant such as CsI, KI, PbSe and PbTe will provide high enough density of states (i.e. small enough  $\hbar$  in our model Hamiltonian) to enable efficient rotational excitation. In order to get efficient rotational excitation at a field in-

tensity which is small as possible one should choose a molecule with a sufficiently large dipole moment. Blümel et al. suggested CsI as the most promising candidate. Therefore, rotational excitation of CsI is expected to show a broad step-like probability distribution in the extended case when a CW laser is used (as proposed here) and exponential localization of CsI at  $j=0$  as well as random time evolution when periodic microwave pulses are used as proposed by Blümel, Fishman and Smilansky [23].

This work has been supported by the Deutsche Forschungsgemeinschaft (Sonderforschungsbereich No. 91 and Schwerpunktprogramm Atom-Molekültheorie), the Israeli Academy of Sciences and Humanities, by the Fund for Encouragement of Research at Technion, and by the S. and N. Grand Research Fund. We are grateful to the RHRK at Kaiserslautern for allocating computing time on the vector machine. It is a pleasure to thank S. Fishman, K. Życzkowski, and A.R. Kolovsky for helpful discussions.

## References

- Gutzwiller, M.C.: *Chaos in classical and quantum mechanics*. Berlin, Heidelberg, New York: Springer 1990
- Haake, F.: *Quantum signatures of chaos*. Berlin, Heidelberg, New York: Springer 1991
- Gay, J.-C.: *Irregular atomic systems and quantum chaos*. Philadelphia: Gordon and Breach 1992 (which is an extension of the collection of articles first appearing in *Comm. At. Mol. Phys.*: **25** (1990))
- Chaos and quantum physics, Les Houches 1989, Giannoni, M.-J., Voros, A., Zinn-Justin, J. (eds.). Amsterdam: North-Holland 1991; Quantum chaos, Trieste 1990, Cerdeira, H.A., Ramaswamy, R., Gutzwiller, M.C., Casati, G. (eds.). Singapore: World Scientific 1991; Quantum chaos - quantum measurement, Copenhagen 1991, Cvitanović, P., Percival, I., Wirzba, A. (eds.). Dordrecht: Kluwer 1992; Quantum non-integrability, Feng, D.H., Yuan, J.-M. (eds.). Singapore: World Scientific 1992
- Pechukas, P.: *Phys. Rev. Lett.* **51**, 943 (1983); Berry, M.V.: *Ann. Phys. (N.Y.)* **131**, 163 (1984); Berry, M.V., Tabor, M.: *Proc. Roy. Soc. Lond. A* **356**, 375 (1972); Bohigas, O., Giannoni, M.J., Schmit, C.: *Phys. Rev. Lett.* **52**, 1 (1984); Berry, M.V., Robnik, M.: *J. Phys. A* **17**, 2413 (1984)
- Casati, G., Chirikov, B.V., Izrailev, F.M., Ford, J.: In: *Lecture Notes in Physics*, Vol. 93, p. 334. Berlin, Heidelberg, New York: Springer 1979
- Chirikov, B.V., Izrailev, F.M., Shepelyansky, D.L.: *Sov. Sci. Rev. C2*, 209 (1981)
- Fishman, S., Grempl, D.R., Prange, R.E.: *Phys. Rev. Lett.* **49**, 509 (1982)
- Grempl, D.R., Prange, R.E., Fishman, S.: *Phys. Rev. A* **29**, 1639 (1984)
- Izrailev, F.M.: *Phys. Rev. Lett.* **56**, 541 (1986)
- Brivio, G.P., Casati, G., Perotti, L., Guarneri, I.: *Physica D* **33**, 51 (1988)
- Blümel, R., Smilansky, U.: *Phys. Rev. Lett.* **52**, 51 (1984)
- Casati, G., Chirikov, B.V., Shepelyansky, D.L.: *Phys. Rev. Lett.* **53**, 2525 (1984)
- Leopold, J.G., Richards, D.: *Phys. Rev. A* **38**, 2660 (1988)
- Casati, G., Chirikov, B.V., Izrailev, F.M., Ford, J.: In: *Lecture Notes in Physics*, Vol. 93, p. 334. Berlin, Heidelberg, New York: Springer 1979; Chirikov, B.V., Izrailev, F.M., Shepelyansky, D.L.: *Sov. Sci. Rev. C2*, 209 (1981); Fishman, S., Grempl, D.R., Prange, R.E.: *Phys. Rev. Lett.* **49**, 509 (1982); Grempl, D.R., Prange, R.E., Fishman, S.: *Phys. Rev. A* **29**, 1639 (1984); Brivio, G.P., Casati, G., Perotti, L., Guarneri, I.: *Physica D* **33**, 51 (1988)
- See the discussion of the kicked top in [1], Chapt. 7.6
- Ben-Tal, N., Moiseyev, N., Korsch, H.J.: *Phys. Rev. A* **46**, 1663 (1992)
- Ben-Tal, N., Moiseyev, N., Fishman, S., Bensch, F., Korsch, H.J.: *Phys. Rev. E* **47**, 1646 (1993)
- Bensch, F., Korsch, H.J., Mirbach, B., Ben-Tal, N.: *J. Phys. A* **25**, 6761 (1992)
- Berry, M.V., Balazs, N.L., Tabor, M., Voros, A.: *Ann. Phys. (N.Y.)* **122**, 26 (1979); Korsch, H.J., Berry, M.V.: *Physica D* **3**, 627 (1981)
- Radons, G., Geisel, T., Rubner, J.: *Adv. Chem. Phys.* **73**, 891 (1989)
- Boorstein, J.L., Uzer, T.: *Can. J. Chem.* **70**, 488 (1992)
- Blümel, R., Fishman, S., Smilansky, U.: *J. Chem. Phys.* **84**, 2604 (1986)
- Escande, D.F., Doveil, F.: *Phys. Lett. A* **83**, 307 (1981); Escande, D.F.: *Phys. Rep.* **121**, 165 (1985); Bialek, J., Schmidt, G., Wang, B.H.: *Physica D* **14**, 265 (1985)
- Croquette, V., Poitou, C.: *Physique* **42**, L537 (1981); Meissner, H., Schmidt, G.: *Am. J. Phys.* **54**, 800 (1986); Briggs, K.: *Am. J. Phys.* **55**, 1083 (1987)
- Berman, G.B., Zaslavsky, G.M., Kolovsky, A.R.: *Sov. Phys. JETP* **54**, 272 (1981); Berman, G.B., Zaslavsky, G.M., Kolovsky, A.R.: *Phys. Lett. A* **87**, 152 (1982); Berman, G.B., Kolovsky, A.R.: *Phys. Lett. A* **95**, 15 (1983); Berman, G.B., Zaslavsky, G.M., Kolovsky, A.R.: *Sov. Phys. JETP* **61**, 925 (1985); Berman, G.B., Vlasova, O.F., Izrailev, F.M.: *Sov. Phys. JETP* **66**, 269 (1987); Kolovsky, A.R.: *Phys. Lett. A* **157**, 474 (1991)
- Chirikov, B.V.: *Phys. Rep.* **52**, 263 (1979)
- Breuer, H.P., Dietz, K., Holthaus, M.: *Physica D* **46**, 317 (1990)
- Graham, R., Keymer, J.: *Phys. Rev. A* **44**, 6281 (1991); Graham, R., Schüdtmann, M., Shepelyansky, D.L.: *Phys. Rev. Lett.* **67**, 255 (1991)
- Perez, A.: *Quantum chaos*, Trieste 1990, Cerdeira, H.A., Ramaswamy, R., Gutzwiller, M.C., Casati, G. (eds.), p. 73. Singapore: World Scientific 1991
- Berman, G.B., Vlasova, O.F., Izrailev, F.M.: *Sov. Phys. JETP* **66**, 269 (1987)
- Berman, G.B., Zaslavsky, G.M., Kolovsky, A.R.: *Phys. Lett. A* **87**, 152 (1982); Berman, G.B., Kolovsky, A.R.: *ibid.* **95**, 15 (1983)
- Schinke, R., Bowman, J.M.: In: Bowman, J.M. (ed.), *Molecular collision theory*, Berlin, Heidelberg, New York: Springer 1983; Korsch, H.J., Ernesti, A.: *J. Phys. B* **25**, 3565 (1992)
- Berry, M.V., Balazs, N.L.: *J. Phys. A* **12**, 625 (1979); Berry, M.V., Balazs, N.L., Voros, A.: *Ann. Phys. (N.Y.)* **122**, 26 (1979); O'Connor, P.W., Tomsovic, S., Heller, E.J.: *Physica D* **55**, 340 (1992)
- Ben-Tal, N., Moiseyev, N., Leforestier, C., Kosloff, R.: *J. Chem. Phys.* **94**, 7311 (1991)
- Zel'dovich, Ya.B.: *Sov. Phys. JETP* **24**, 1006 (1967); Ritus, V.I.: *Sov. Phys. JETP* **24**, 1041 (1967)
- Howland, J.S.: *Ann. Inst. Henri Poincaré, Phys. Theor.* **50**, 309 (1989); *ibid.*, 325
- Haake, F., Kus, M., Scharf, R.: *Z. Phys. B* **65**, 381 (1987)
- Diltrich, T., Smilansky, U.: *Nonlinearity* **4**, 59 (1991); *ibid.* **85**
- Wooters, W.K.: *Found. Phys.* **20**, 1365 (1990)
- Zimmermann, Th., Köppel, H., Coderbaum, L.S.: *J. Chem. Phys.* **91**, 3934 (1989)
- Pechukas, P.: *Chem. Phys. Lett.* **86**, 553 (1982); *J. Phys. Chem.* **88**, 4823 (1984); *J. Math. Phys.* **25**, 532 (1984); Wilkie, J., Brumer, P.: *Phys. Rev. Lett.* **67**, 1185 (1991)
- Levine, R.D.: *Adv. Chem. Phys.* **70**, 53 (1988)
- Życzkowski, K.: *J. Phys. A* **23**, 4427 (1990); Życzkowski, K.: In: *Quantum chaos*, Trieste 1990, Cerdeira, H.A., Ramaswamy, R., Gutzwiller, M.C., Casati, G. (eds.), p. 153. Singapore: World Scientific 1991
- Jones, K.R.W.: *J. Phys. A* **23**, L1247 (1990)
- Alhassid, Y., Levine, R.D.: *Phys. Rev. Lett.* **57**, 2879 (1986); Alhassid, Y., Feingold, M.: *Phys. Rev. A* **39**, 374 (1989); Kus, M., Życzkowski, K.: *Phys. Rev. A* **44**, 956 (1991)
- Feingold, M., Moiseyev, N., Peres, A.: *Chem. Phys. Lett.* **117**, 344 (1985); Feingold, M., Peres, A.: *Phys. Rev. A* **34**, 591 (1986); Alhassid, Y., Levine, R.D.: *Phys. Rev. Lett.* **57**, 2879 (1986)
- Kus, M., Mostowski, J., Haake, F.: *J. Phys. A* **21**, L1073 (1988)